Spectro-electrochemical probing of intrinsic and extrinsic processes in exciton recombination in I-III-VI_2 nanocrystal

Valerio Pinchetti,[a] Monica Lorenzon, [a] Hunter McDaniel, [b,c] Roberto Lorenzi, [a] Francesco Meinardi,[a] Victor I. Klimov[c] and Sergio Brovelli*,[a]

[a] *Dipartimento di Scienza dei Materiali, Università degli Studi di Milano-Bicocca, via R. Cozzi 55, I-20125 Milano, Italy*
[b] *UbiQD, Los Alamos, New Mexico, 87544, USA*
[c] *Chemistry Division and Center for Advanced Solar Photophysics, Los Alamos National Laboratory, Los Alamos, New Mexico 87545, USA*

Corresponding Author: sergio.brovelli@unimib.it (Telephone:+39 02 6448-5027).

ABSTRACT

Ternary $CuInS_2$ nanocrystals (CIS NCs) are attracting attention as non-toxic alternatives to heavy metal–based chalcogenides for many technologically relevant applications. The photophysical processes underlying their emission mechanism are, however, still under debate. Here we address this problem by applying, for the first time, spectro-electrochemical methods to core-only CIS and core/shell CIS/ZnS NCs. The application of an electrochemical potential enables us to reversibly tune the NC Fermi energy and thereby control the occupancy of intra-gap defects involved in exciton decay. The results indicate that, in analogy to copper-doped II-VI NCs, emission occurs via radiative capture of a conduction-band electron by a hole localized on an intragap state likely associated with a Cu-related defect. We observe the increase in the emission efficiency under reductive electrochemical potential, which corresponds to raising the Fermi level, leading to progressive filling of intragap states with electrons. This indicates that the factor limiting the emission efficiency in these NCs is nonradiative electron trapping, while hole trapping is of lesser importance. This observation also suggests that the centers for radiative recombination are Cu^{2+} defects (preexisting and/or accumulated as a result of photo-conversion of Cu^{1+} ions) as these species contain a pre-existing hole without the need for capturing a valence-band hole generated by photoexcitation. Temperature-controlled photoluminescence experiments indicate that the intrinsic limit on the emission efficiency is imposed by multi-phonon non-radiative recombination of a band-edge electron and a localized hole. This process affects both shelled and unshelled CIS NCs to a similar degree, and it can be suppressed by cooling samples to below 100K. Finally, using experimentally measured decay rates, we formulate a model that describes the electrochemical modulation of the PL efficiency in terms of the availability of intragap electron traps as well as direct injection of electrons into the NC conduction-band, which activates nonradiative Auger recombination, or electrochemical conversion of the Cu^{2+} states into the Cu^{1+} species that are less emissive due to the need for their "activation" by the capture of photogenerated holes.

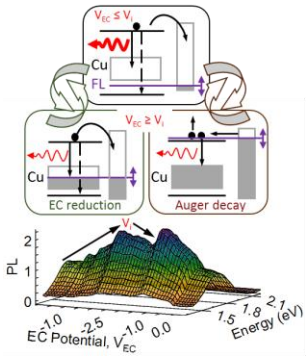

KEYWORDS: *Nanocrystal, quantum dot, $CuInS_2$, spectro-electrochemistry, I-III-VI_2, Cu-related defect, trapping, temperature-dependent photoluminescence*

Colloidal semiconductor nanocrystals (NCs) are a widely investigated class of solution-processable functional materials with size-tunable optical properties that are emerging as active components in many technologies from LEDs[1−3] and lasers[1,4] to photovoltaics,[5,6] sensing,[7,8] and bioimaging.[9,10] Recently, toxicity and environmental concerns have led to strict regulations around the well-known classes of cadmium- and lead-based chalcogenide systems, which has boosted the interest in heavy-metal-free alternatives, such as I−III−VI_2 ternary NCs featuring technologically interesting optical properties, such as size-tunable bandgap from visible to NIR,[11−13] intense broadband absorption[14,15] and efficient Stokes-shifted luminescence.16−19 In addition, they can be fabricated in large quantities via high-throughput, non-injection techniques using inexpensive precursors.[20] NCs of $CuInS_2$ (CIS), $CuInSe_2$ (CISe), and their alloys $CuInSe_xS_{2-x}$ (CISeS) have been successfully used in photocatalysis,[21] sensing,[22] and bioimaging,[23−25] as well as in photonic devices such as LEDs,[26,27] solar cells[28−34] and, more recently, reabsorption-free luminescent solar concentrators.[18,35−37] Because of its technological relevance in photon-management and lighting applications,[38,39] particular attention has been devoted to the elucidation of the origin of the broad,[40,41] strongly Stokes-shifted photoluminescence (PL).[18,42] Recent interpretations suggest the partial forbiddances of optical transitions between the electron and hole ground states due to the tetragonal symmetry of the crystal lattice[43] or exciton self-trapping processes[44] as possible mechanisms. A more commonly accepted emission mechanism, however, is radiative recombination of a photoexcited band-edge electron and a hole residing in an intragap state[16,18,41,42,45−51] often associated with off-stoichiometric effects that have been shown to enhance the emission efficiency.[11,49,52,53]

To date, the nature of the intragap state in CIS NCs is not fully understood and is often related[17,42,54] to optically active centers responsible for the non-resonant long-lived PL in copper-doped II−VI semiconductors whose optical and magnetic properties are very similar to those of ternary I−III−VI compounds.[42,55−62] In copper-doped II−VI semiconductors, the 3d states of the Cu impurities introduce a fairly deep intragap acceptor level near the NC valence band (VB).[63−65] The crystal field of the host lattice splits the degeneracy of the 3d state into two distinct sublevels within the gap, the higher in energy being 6-fold degenerate and conventionally labeled as t, whereas the lower level is 4-fold degenerate and labeled e (refs 64 and 65). The Fermi energy of the NC determines the occupancy of these states: when the Fermi level is above them, the 3d shell is completely filled, which corresponds to the +1 oxidation state of Cu with electronic configuration $(Ar)^3d^{10}$. When the Fermi level is below the t-state, the electronic configuration becomes $(Ar)^3d^9$, corresponding to the +2 oxidation state of Cu (ref 63). In this latter case, the impurity acts as a paramagnetic acceptor state, which can radiatively capture a conduction band (CB) electron without the need for a photogenerated hole.[56,66−68] On the contrary, capture of a VB hole by the dopant is necessary in order to enable the radiative decay of a CB electron via a Cu^{1+} center.[69,70] Notably, while spectro-electrochemistry (SEC) experiments pointed to a major role of Cu^{2+} species in the emission process of Cu:ZnSe/ CdSe NCs, magnetic circular dichroism (MCD) studies on the same systems revealed that photomagnetism due to sp-d spin-exchange coupling in NCs with +2 copper impurities undergoes strong (up to 100%) enhancement upon UV illumination, suggesting that diamagnetic Cu^{1+} dopants can be photoconverted into paramagnetic Cu^{2+} centers.[59]

The photophysical and structural similarities between Cu-doped II−VI NCs (i.e., CdSe, ZnSe)[44] and I−III−VI_2 NCs, which feature a unit cell composed of two zinc-blende unit cells distorted along the c-axis,[71−73] suggest a similar recombination mechanism also for CIS (or CISeS in general) NCs. Notably, in these NCs the intragap recombination center seems to be a “native” defect, as indicated by the consistency of the optical features exhibited by ternary NCs obtained via di^{ff}erent synthetic techniques.[14,52,53,74−76] Compositional analyses by X-ray photoelectron spectroscopy[75] indicate that

the main oxidation state of copper in CIS NCs and their alloys is +1. Nevertheless, the exact ascription of the copper state responsible for the PL of I−III−VI_2 is still debated with some studies indicating Cu^{1+} as the emissive center,[14,69] whereas other studies point to the presence of small amounts of paramagnetic Cu^{2+} defects (complemented, e.g., by Cu vacancies, V_{Cu}, for charge neutrality)[42] in the NC lattice as the species responsible for the optical and magnetic properties of CIS NCs.[18,42,59] A more recent theoretical study of wurtzite CIS NCs by Macdonald and co-workers suggests that interstitial Cu^0 defects introduce an intragap acceptor state with the localization energy comparable to the experimentally observed Stokes shift.[51] While such charge-neutral Cu species might occur in CIS NCs, a considerable amount of literature points toward the prevailing role of substitutional Cu^{1+} (might occur as an antisite Cu_{In}^{1+}−In_{Cu}^{3+} pair) and Cu2+ (paired, e.g., with VCu) defects[41,42,52,73,77−79] in defining photophysical properties of CIS NCs. In fact, several recent studies seem to suggest that the radiative decay centers are likely Cu^{2+} species at least in some of the samples where the position of the Fermi level favors this type of states.[41,42,80] Furthermore, similar to previous observations for Cu:doped II−VI NCs, Cu^{1+} states can in principle be photoconverted to Cu^{2+} centers upon capture of a VB hole. In this case, the interplay between the hole capture by the Cu^{+} defects and surface traps would determine the sensitivity of the emission efficiency to external hole withdrawing agents. The scenario of Cu^{2+}-mediated luminescence in CIS NCs (due to either pre-existing or photoconverted Cu^{2+} states) is, for example, supported by recent spectroscopic investigations,[17] showing that the main factor controlling the PL efficiency in CIS NCs is nonradiative trapping of photoexcited electrons, whereas hole trapping does not appreciably affect the PL quantum yield. Another piece of evidence in favor of the Cu^{2+} emission mechanism is a quantitative similarity in light-emission properties (including PL spectral and relaxation characteristics) between CIS NCs and Cu-doped ZnSe NCs.[42] The Cu^{2+} character of emissive species in the latter system was indicated by the fact that intragap PL was enhanced when NCs were treated with hole scavengers.[55]

Here, we combine temperature-controlled PL studies and SEC methods to elucidate the emission mechanism in I−III−VI_2 NCs and shed light on the nature of the intragap state involved in the radiative recombination process. We demonstrate that by tuning the position of the Fermi level through the application of an electrochemical (EC) potential, we alter the occupancy of intragap states and thereby reversibly change the NC's emission intensity by promoting/hindering selective carrier trapping in defect sites. The effect of the EC potential is reduced in core/ shell CIS/ZnS NCs compared to core-only structures, which is an expected consequence of suppressed extrinsic nonradiative decay processes due to improved electronic passivation of the CIS−core surfaces by a wide-gap shell[18] that effectively reduces the abundance of intragap traps. Our data show that the PL efficiency of unshelled NCs is strongly enhanced upon raising the Fermi level, which leads to filling (passivation) of electron trapping sites. Because the same conditions lead to activation of additional hole trapping states, this observation indicates that enhanced trapping of photogenerated holes does not diminish the PL efficiency, pointing toward a recombination pathway involving either a pre-existing hole-like Cu^{2+} intragap state or a photogenerated acceptor produced via hole trapping by Cu^{1+} defects occurring on a faster time scale than hole trapping by EC activated surface defects.[42,56] Furthermore, both core-only and core/shell NCs with passivated surfaces show a drop in the PL intensity at the highest negative potentials, which might be associated with either direct injection of electrons into the NC conduction band, which activates nonradiative Auger recombination,[8,81,82] or EC conversion of the Cu^{2+} states into the Cu^{1+} species that are less emissive due to the need for their "activation" by the capture of photogenerated holes.[55] Temperature controlled PL measurements on both shelled and unshelled NCs point to the presence of an intrinsic thermally assisted nonradiative decay process with similar activation energies in both structures. The suppression of this nonradiative pathway at cryogenic temperatures leads to a two-fold

enhancement of the PL quantum yield. Finally, in order to rationalize the SEC observations in terms of competition between the involved recombination channels, we develop a model which links the PL efficiency to the occupancy of intragap traps and also accounts for the possibility of either direct injection of electrons into the NC conduction band or EC reduction of Cu^{2+} centers to Cu^{1+}.

Optical Properties of Core-Only and Core/Shell CIS/ZnS Nanocrystals. The core-only and core/shell CIS/ZnS NCs with ~4 nm side length were synthesized following the route described in ref 18. The transmission electron micrographs are reported in Figures S1 and S2. The optical absorption spectrum and the characteristic Stokes-shifted PL of core-only CIS and core/shell CIS/ZnS NCs are shown in Figure 1a together with the respective PL excitation (PLE) spectra collected at the emission maximum. The spectra of the core/shell NCs are slightly blue-shifted with respect to the respective core-only NCs as typically observed for the situation when the shell growth occurs via cation exchange, which leads to the effective reduction of the emissive core accompanied by the increase in the degree of spatial confinement.[16] In both cases, the PLE spectra follow nearly perfectly the respective absorption profile, which confirms that the PL is excited by intrinsic electronic transitions of the NCs. The PL quantum yield, as measured with an integrating sphere, is Φ_{PL} = 5 ± 1% and Φ_{PL} = 35 ± 3% for the core-only and the core/shell NCs, respectively. The increase in the PL efficiency in the case of the core/shell sample indicates the effectiveness of electronic passivation of the core surface by a wide-gap ZnS layer which creates a type-I energetic barrier.[18,41,83]

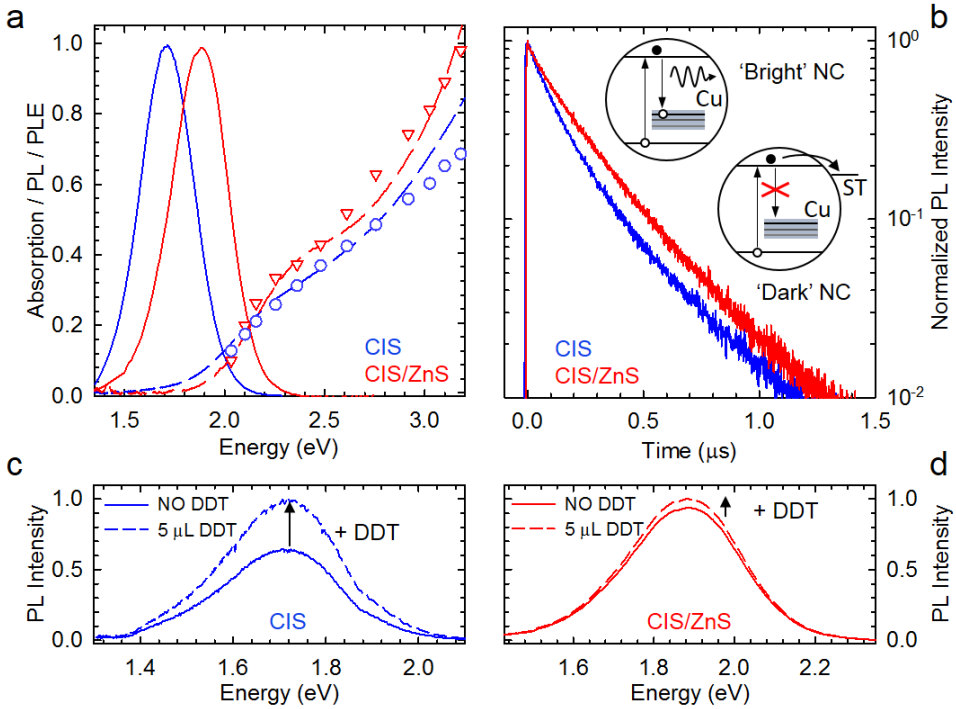

Figure 1 *(a) Absorption (dashed lines) and photoluminescence (PL) spectra (solid lines) of CIS core-only (blue lines) and core/shell CIS/ZnS (red lines) NCs in toluene. The PL excitation (PLE) spectra are shown as blue circles for CIS NCs (collected at 1.7 eV) and red triangles for CIS/ZnS NCs (collected at 1.9 eV). (b) PL decay traces of the same solutions collected at the respective PL maxima. Inset: A simplified structure of the band-edge electronic states in CIS NCs responsible for optical absorption and PL. Light absorption is dominated by optical transitions between intrinsic quantized states, while the PL arises from the radiative capture of a band-edge electron*

by an intragap state associated with a Cu-related defect acting as the emission center. The absence of electron trapping channels leads to 'bright' NCs whereas fast electron transfer to surface traps (ST) leads to non-emissive 'dark' particles in the ensemble. PL spectra of (c) CIS NCs and (d) CIS/ZnS NCs in the absence (solid lines) and in the presence (dashed lines) of the dodecanethiol, DDT (5 μL DDT per mL solution), a known hole scavenger. The PL spectra of both samples are normalized to their value after the addition of DDT. All PL measurements were performed using pulsed 3.1 eV excitation (per-pulse excitation fluence is 0.5 μJ/cm^2).

As shown in Figure 1b, the ∼7-fold enhancement of Φ_{PL} upon shelling the CIS NCs with ZnS occurs without significant changes in the PL decay dynamics that for both systems is slightly multiexponential in agreement with previous results.[11,16−18] The effective PL lifetimes, extracted as the time for which the PL signal drops by a factor of e, are ∼200 and ∼175 ns for the core/shell and core-only NCs, respectively. This indicates that the deposition of the ZnS shell suppresses rapid (unresolved in our measurements) nonradiative surface trapping that occurs prior to radiative decay, while leaving the spatial overlap between the electron and hole wave functions nearly unaltered. We note that surface trapping could, in principle, affect both "hot" and relaxed band-edge carriers, however, a close match between the PLE and the absorption spectra (Figure 1a) indicates that the trapping process involves primarily carriers close to the NC's band edges. The lower emission yield of the CIS core-only sample with respect to core/shell particles is, therefore, likely due to a larger fraction of nonemissive ("dark") NCs, in which electron surface trapping outpaces radiative decay, compared to the fraction of emissive "bright" NCs that do not contain "fast" electron traps (inset of Figure 1b).

SEC experiments reported in the following sections can also be explained using the above two subensemble model. In fact, they demonstrate that the application of an EC potential reversibly converts "dark" NCs into "bright" ones and vice versa by passivating/activating electron surface traps. In II−VI NCs doped with Cu^{2+}, PL quenching has been mostly ascribed to rapid electron trapping,[55] while trapping of VB holes has been considered to have a minor role due to the ability of a Cu^{2+} acceptor state to directly capture a CB electron via a radiative transition.[56] Indeed, the addition of 1-dodecanethiol (DDT), which has been observed to quench the PL from CdSe NCs[84] due to rapid extraction of photogenerated VB holes, leads to brightening of Cu:ZnSe/CdSe NCs resulting from the passivation of electron accepting surface defects.[56] A similar behavior has been also observed for CdTe NCs,[84,85] whose band-edge holes reside above the redox level of DDT and thus cannot be reduced by it. Interestingly, similarly to Cu-doped NCs, the exposure of CIS NCs to DDT enhances their PL efficiency, although their VB energy (E_{VB} ∼−6.26 eV)[20,85,86] is comparable to CdSe NCs (E_{VB} ∼−6.1 eV).[84,87] In Figure 1, we display the PL spectra of both unshelled (panel c) and shelled (panel d) samples recorded in the absence and in the presence of DDT (5 μL in 1 mL of NCs solution). The addition of DDT to core-only CIS NCs leads to strong 60% enhancement of the PL efficiency suggesting that, as in Cu-doped II−VI NCs, the main emission intensity-limiting mechanism is electron trapping,[17] which becomes suppressed upon exposure to electron-donating DDT molecules.[84] On the other hand, the absence of PL quenching due to rapid hole withdrawal is indicative of an emission process involving an intragap acceptor state, which is occupied with a preexisting hole, or act as a very fast trap for photogenerated VB holes outcompeting hole extraction by DDT. These two types of behaviors can be expected, respectively, for Cu^{2+} and Cu^{1+} intragap defects. The addition of DDT also improves the PL efficiency of CIS/ZnS NCs, although, in this case, the enhancement is less than 10% (Figure 1d). The diminished effect of electron-donating species in this case is due to already effective passivation of surface electron traps by the ZnS layer.

Temperature-Controlled Photoluminescence Experiments. To quantify the effect of nonradiative decay channels in our NCs and to investigate the intrinsic radiative decay rates in the "bright" particles in both the CIS and CIS/ZnS NCs ensembles, we perform temperature-controlled PL experiments. In Figure 2 panels a,b and panels c,d, we report the PL spectra and the decay curves at decreasing temperature of CIS and CIS/ ZnS NCs, respectively. Both samples show monotonic enhancement of the emission intensity from T = 300 K to T = 70 K.

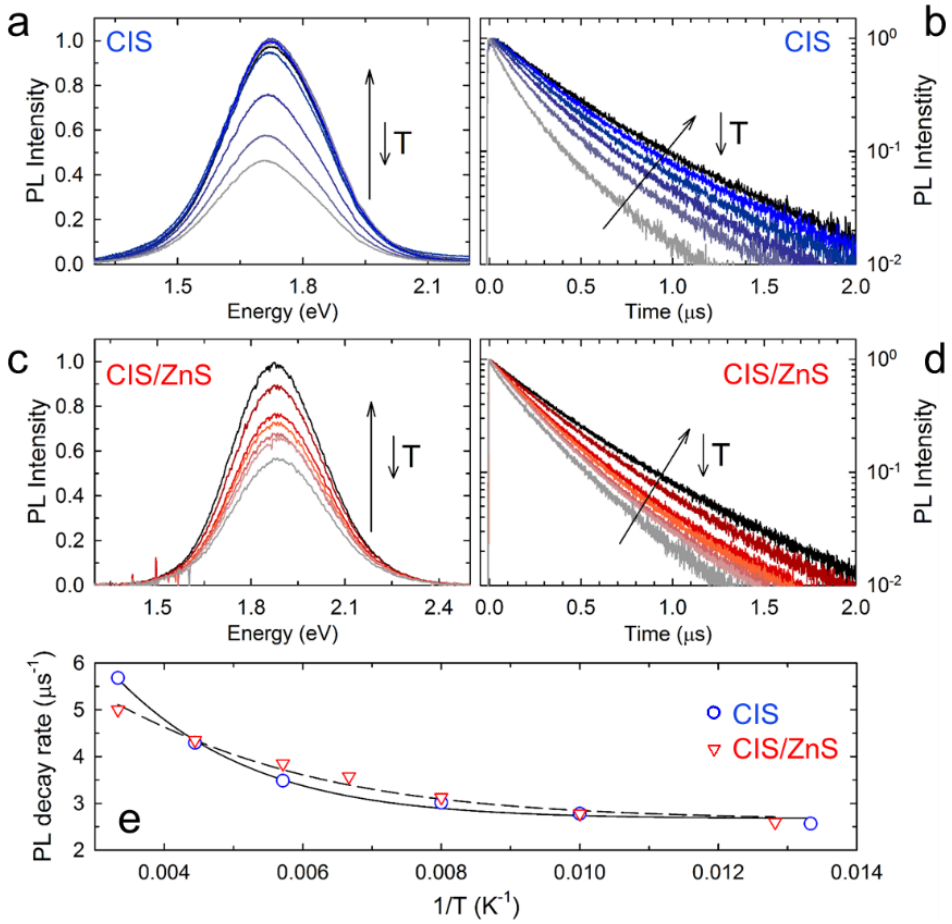

Figure 2*.(a,c) PL spectra and (b,d) time-resolved PL traces for core-only CIS NCs and CIS/ZnS as a function of decreasing temperature as indicated by the arrows. The PL spectra are normalized to their value at T = 77 K. (e) Effective decay rates ($\tilde{k}$) extracted from the PL traces in b and d as a function of T−1 (blue circles for CIS NCs and red triangles for CIS/ZnS). The respective fits to eq 1 are shown as a solid line for the CIS NCs and as a dashed line for CIS/ZnS NCs. The zero-delay PL intensities normalized to their respective values at 70 K are shown in the inset. The same color scheme applies throughout the figure.*

At any temperature, both PL dynamics are slightly multiexponential, as typically observed for CIS NCs.[11,16–18] At T = 300 K, the effective decay lifetime is $\tilde{\tau}$ = 200 ns (corresponding to an effective decay rate $\tilde{k} = 1/\tilde{\tau}$ = 5 μs^{-1}) and $\tilde{\tau}$ = 175 ns ($\tilde{k}$ = 5.7 μs^{-1}) for CIS and CIS/ZnS NCs, respectively. In both cases $\tilde{\tau}$ increases to ~370 ns ($\tilde{k}$ = 2.7 μs^{-1}) at T = 70 K. Importantly, as evident from Figure 2b,d and additionally highlighted in the inset of Figure 2e, no appreciable effect of temperature is observed for the zero-delay PL intensity, indicating that ultrafast electron trapping is virtually temperature-independent.[88] This further suggests that the relative fraction of "bright"

versus "dark" NCs in the ensemble is unaltered by temperature. On the other hand, changes in temperature affect the decay dynamics in the sub-ensemble of "bright" NCs. This observation, together with the strong resemblance between the temperature dependent trends observed for core-only and core/shell NCs, suggest that the nonradiative process competing with radiative decay might involve phonon-assisted trapping of electrons at internal structural defects. Accordingly, the effective decay rates of CIS and CIS/ZnS NCs follow a very similar trend with decreasing temperature. The evolution of the effective decay rate is shown in Figure 2e together with the respective fit to the equation: $\tilde{k} = k_{RAD} + k_{NRAD}(T)$, that neglects ultrafast surface electron trapping and describes the nonradiative decay rate by the standard displaced harmonic oscillator model[89]

$$k_{NRAD}(T) = A * exp(-E_A/(k_B T)). \qquad (1)$$

Through this fit, we obtain essentially the same effective radiative decay rate (k_{RAD}) for CIS and for CIS/ZnS NCs ($k_{RAD} = 2.58 \times 10^6\ s^{-1}$ and $k_{RAD} = 2.61 \times 10^6\ s^{-1}$, respectively) and activation energies for the nonradiative decay of 56 meV for CIS NCs and of 40 meV for CIS/ZnS NCs. Using the obtained radiative and nonradiative decay rates, we finally use the equation $\Phi_{PL,BRIGHT} = k_{RAD}/\tilde{k}$ to quantify the room temperature PL efficiency of the "bright" NCs in the two ensembles that is found to be $\Phi_{PL,BRIGHT}$ ~50% for both core-only and core/shell CIS/ZnS NCs. Considering that the overall PL quantum yields are 5 ± 1% and 35 ± 3% for the CIS and the CIS/ZnS sample, respectively, this indicates that the fractions of "bright" particles in the core-only sample is ~10%, and it increases to 70% upon shelling.

Spectro-electrochemistry Experiments. To gain a deeper insight into the effect of intragap states on the radiative and nonradiative recombination in CIS and CIS/ZnS NCs, we have performed SEC measurements, wherein we tune the Fermi level in a controlled and reversible fashion through the application of an EC potential.[55,81,90] Figure 3a shows a schematic depiction of the experimental setup used in the SEC measurements. A working electrode comprises an ITO-coated quartz substrate covered by a film of sintered ZnO particles (~50 nm diameter) and a thin layer of NCs; silver and platinum wires are used as reference and counter-electrodes, respectively. We start our measurements by applying a negative EC potential, which corresponds to raising the Fermi level in the NC film leading to progressive passivation (activation) of the surface electron (hole) traps (ET and HT in Figure 3a, respectively). In Figure 3b, we report the complete set of PL spectra of CIS NCs under application of a negative EC potential (V_{EC}) scanned from 0 to −2.5 V and then back to 0 V (a complete set of PL spectra of CIS/ZnS NCs is shown in Figure S3). To quantify the effect of the EC potential on the PL intensity of both the core and core/shell NCs, in Figure 3c we plot the respective integrated PL intensities as a function of the EC potential normalized to their values at V_{EC} = 0 V. In the case of CIS NCs (blue circles, Figure 3c), no noticeable changes in the PL intensity occur at the initial stage of the potential ramp (up to V_{EC} = −1 V). This is common in SEC measurements of colloidal nanostructures that use ITO/ZnO electrodes[8,55,90,91] to suppress PL quenching by energy- and/or charge-transfer from the NCs to the ITO.[90,92] The introduction of the additional ZnO spacer along with the presence of insulating surface ligands can lead to an appreciable attenuation of the actual shift of the Fermi level compared to the nominal applied EC potential.[93] At negative potentials above V_{EC} = −1 V, we observe strong PL brightening as indicated by ~150% enhancement of the PL intensity for V_{EC} = −2 V. The effect of the reductive EC potential is similar to that of the exposure to DDT (Figure 1c), which points to the similarity of the underlying mechanisms that in both cases involve gradual

filling of electron trap sites on the NC surface, leading to the progressive increase in the fraction of "bright" NCs versus the "dark" non-emissive ones.

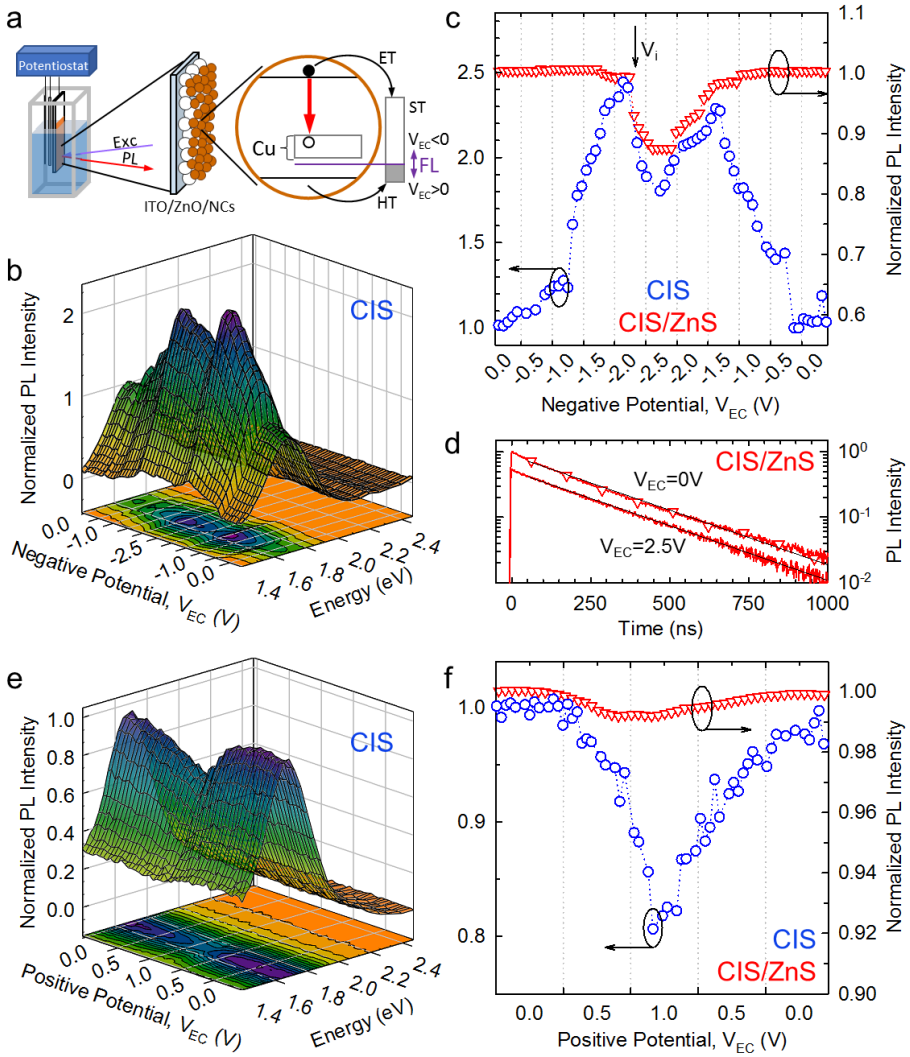

Figure 3 *(a) Schematics of the SEC setup and the effect of the EC potential on the PL intensity of CIS NCs due to filling/emptying of surface traps (ST) in response to changes in the position of the Fermi level (FL; purple line). (b) Series of core-only CIS NCs PL spectra (5s acquisition/frame) during a stepwise scan of the negative EC potential from V_{EC}=0 V to -2.5V (each 0.5 V step, 30 s). (c) Integrated PL intensity of CIS NCs (blue circles, left y-axis) and CIS/ZnS NCs (red triangles, right y-axis) under applied negative EC potential based on the spectra in 'b' and Fig.S1. Both dependences are normalized to their values at V_{EC}=0 V. (d) Time-resolved PL traces of CIS/ZnS NCs at V_{EC}=0 V and -2.5 V. (e) Series of PL spectra (5s acquisition/frame) of CIS NCs during a stepwise scan of the positive EC potential from V_{EC}=0 V to 1 V (0.5 V step, 30 s). (f) Integrated PL intensities for CIS NCs (blue circles, left y-axis) and CIS/ZnS NCs (red triangles, right y-axis) as a function of applied positive EC potential. Both dependences are normalized to their values at V_{EC}=0 V. All measurements are performed using pulsed 3.1 eV excitation with fluence of 10 nJ/cm^2 .*

Accordingly, the PL decay dynamics (Figure S4) shows an appreciable enhancement of its zero delay intensity and only a minor change of the PL lifetime, which confirms that surface electron trapping is very fast (unresolved in these measurements) and occurs prior to radiative decay. Importantly, the concomitant activation of hole traps occurring for raising Fermi energy does not affect the PL intensity, indicating that in the studied CIS NCs the emission process is nearly independent of hole trapping. This is consistent with a scenario in which radiative recombination of CB electrons occurs via holelike Cu^{2+} centers, either already present in the ground state (due, e.g., to sample off-stoichiometry) or induced by transient photooxidation of Cu^{+} sites by capture of VB holes occurring faster than nonradiative trapping by surface defects. Upon reaching a potential of −2 V, the trend in the dependence of the PL intensity versus V_{EC} reverses, and we observe a stepwise ∼20% drop in the PL signal at $V_{EC} = -2.5$ V.

The core/shell CIS/ZnS NCs do not show initial electrochemically induced PL brightening (red triangles, Figure 3c) due to already effective passivation of surface electron traps by the ZnS shell, as was discussed earlier in the context of experiments involving titration with DDT. However, as in the case of coreonly structures, application of a strongly reducing potential ($|V_{EC}| > 2$ V) also leads to the appreciable (∼15%) PL quenching. For both the core-only and core/shell NCs, we observe a full recovery of the initial PL intensity upon returning back to the zero EC potential, suggesting that the observed PL quenching is not caused by any permanent chemical degradation of the NCs.

The sudden drop in the PL intensity at high negative EC potentials is consistent with previous observations for Cu-doped II−VI NCs[55] in which it was ascribed to the EC-induced conversion (reduction) of Cu^{2+} centers into Cu^{+} in the NCs subensemble in which the position of the Fermi level favors the incomplete filling of the copper d electronic shell. Cu^{+} species can participate in the radiative decay only after capturing a photogenerated VB hole, a necessary step that is rendered less efficient under increasing reductive potentials due to the increase in the abundance of active hole traps competing with the Cu^{1+} centers for the photoinjected hole. As a result, a progressive Cu^{2+}-to-Cu^{1+} conversion for increasingly negative V_{EC} can indeed lead to PL dimming without changes in the PL decay dynamics independently of the original oxidation state of the Cu ion. This picture seems to be consistent with observations for CIS/ZnS NC reported in Figure 3d. Specifically, the recorded PL time transients show a drop of the zero-delay PL intensity upon increasing V_{EC} from 0 to −2.5 V, however, the PL lifetime remains unaltered. Similar observations (although somewhat distorted by nonradiative electron trapping) are reported in Figure S4 for CIS NCs.

While the above scenario is plausible, there is also an alternative (or additional) mechanism, which can lead to PL dimming at high negative potential. This mechanism is direct electron injection into the NC conduction band, which would activate nonradiative Auger recombination through the so-called negative trion pathway,[82] that is, the process where the energy released in the exciton recombination is transferred to another electron coexisting in the NC. Such a process, occurring between 30 and 300 ps in CIS NCs,[79,94] would render a portion of the NC population nonemissive, resulting in early time dimming of the PL amplitude unresolved in the PL decay measurements in Figure 3d, while leaving the dynamics of emissive NCs unmodified. The uncertainty in the exact nature of PL quenching process relates to the uncertainty in the absolute magnitude of the Fermi level shift for a given EC potential. Specifically, the interpretation of experimental data of ref.[55] was made under the assumption that the division coefficient between an applied V_{EC} and the resulting shift of the Fermi level was large ($f \sim 20$), therefore, despite large variations in V_{EC}, the actual modulation of the Fermi level was considerably smaller. However, for

a highly conductive ZnO layer the division factor can become greater, which might allow for electron injection into the NC under sufficiently larger negative EC potentials. For example, this condition has been realized in SEC experiments on undoped CdSe/CdS NCs, in which direct injection of electrons in the NC conduction band was achieved at V_{EC} corresponding to half the NC band gap energy ($f \sim 1$),[7,95] consistently with the mid-gap position of the Fermi level in intrinsic semiconductors. The possibility of this process along with the Cu^{2+}-to-Cu^{1+} conversion will be discussed in more quantitative terms in the next section where we conduct modeling of the effect of the EC potential on the PL intensity. On the other hand, since the applied EC potentials are of the order of a few Volts, we exclude exciton dissociation by electric field[96,97] as a potential cause of the observed PL drop.

We next investigate the effect of a positive EC potential on the two NC systems. In Figure 3e, we report the complete set of PL spectra of CIS NCs under positive EC potential up to V_{EC} = +1 V (in Figure S5 we report the analogous plot for the CIS/ZnS NCs). To highlight the effect of lowering the Fermi level, in Figure 3f we show the integrated PL intensity as a function of the cyclic stepwise scan of the positive EC potential. Between V_{EC} = 0 V and V_{EC} = +0.25 V, we observe no measurable modulation of the PL intensity for both samples. Upon increasing the potential to V_{EC} = +1 V, the PL intensity drops by ~20% for the core-only CIS NCs and is nearly constant (<1% drop) for the CIS/ZnS systems (note the different y-scales for core-only and core/shell NCs). This behavior is a continuation of the trend observed for the negative V_{EC} and it is consistent with the progressive activation of intragap traps under oxidative potentials that deplete the CIS NCs of photogenerated electrons to a larger degree than in shelled CIS/ZnS NCs. Accordingly, the early time PL dynamics of CIS NCs (Figure S6) becomes faster upon raising the positive potential to V_{EC} = 1 V. In contrast, the PL dynamics of CIS/ZnS NCs is essentially unaffected by the positive EC potential (Figure S7). As in the case of the negative potential, the PL intensity of both types of samples fully recovers when the EC potential is brought back to V_{EC} = 0 V, indicating no permanent oxidation of the NC surfaces.

Model for Analyzing the Spectro-electrochemical Responses. To rationalize the SEC data, we use a model that links the total PL efficiency to the occupancy of intragap electron traps that can be activated (passivated) by lowering (raising) the Fermi level through the application of an EC potential. The scheme of the decay channels determining Φ_{PL} is depicted in the top panel of Figure 4a, where electron trapping (rate k_{ET}) takes place much faster than radiative capture of photogenerated electrons by intragap hole-like states (rate k_{RAD}); the latter process competes with a nonradiative thermal recombination process (rate k_{NRAD}) as discussed in temperature-controlled PL measurements in Figure 2.

Because hole trapping plays a minor role in the emission process in our NCs, as it is inconsequential for dots with groundstate Cu^{2+} sites and is arguably slower than hole capture by emissive centers in dots with prevailing Cu^{+} defects, we neglect this process in our SEC model. To account for the effect of the EC potential on the occupancy of surface traps, we assume that the traps are distributed in energy across the NC ensemble forming a "trap band" with width N_0. We also assume that the NCs are characterized by a common Fermi level, which determines the trap occupancy (n_0 per individual NC) in the absence of photoexcitation. The rate of electron trapping is determined by the fractions of "dark" (F_D) and "bright" (F_B) NCs that are connected to V_{EC} by $F_D = (N_0 - n_0 + \gamma V_{EC})/N_0$ and $F_B = 1 - F_D$, where γ is the attenuation factor expressed in units of [V^{-1}] between the applied V_{EC} and the resulting shift of the Fermi level. The model further considers the availability of intragap states for radiative decay of photogenerated electrons, which,

consistently with the broad emission line width of CIS NCs[40,55] are described through an "acceptor band". Within the scenario of direct electron injection in intragap defects leading to EC $Cu^{2+} \rightarrow Cu^{+}$ reduction that would imply a strongly attenuated V_{EC} (lower left panel in Figure 4a), the width of such acceptor band, P, is assumed constant ($P = P_0$) for any V_{EC} below the injection potential V_i, which corresponds to the situation in which the Fermi level reaches the lowest-energy Cu^{2+} state under negative bias. For larger negative V_{EC}, electrons are injected directly into the NC intragap states, progressively reducing their number according to $P = P_0 - \gamma \cdot \beta (V_{EC} - V_i)$, where the term β expresses the injection efficiency of electrons in the NCs across the dielectric barrier imposed by the organic ligand shell.

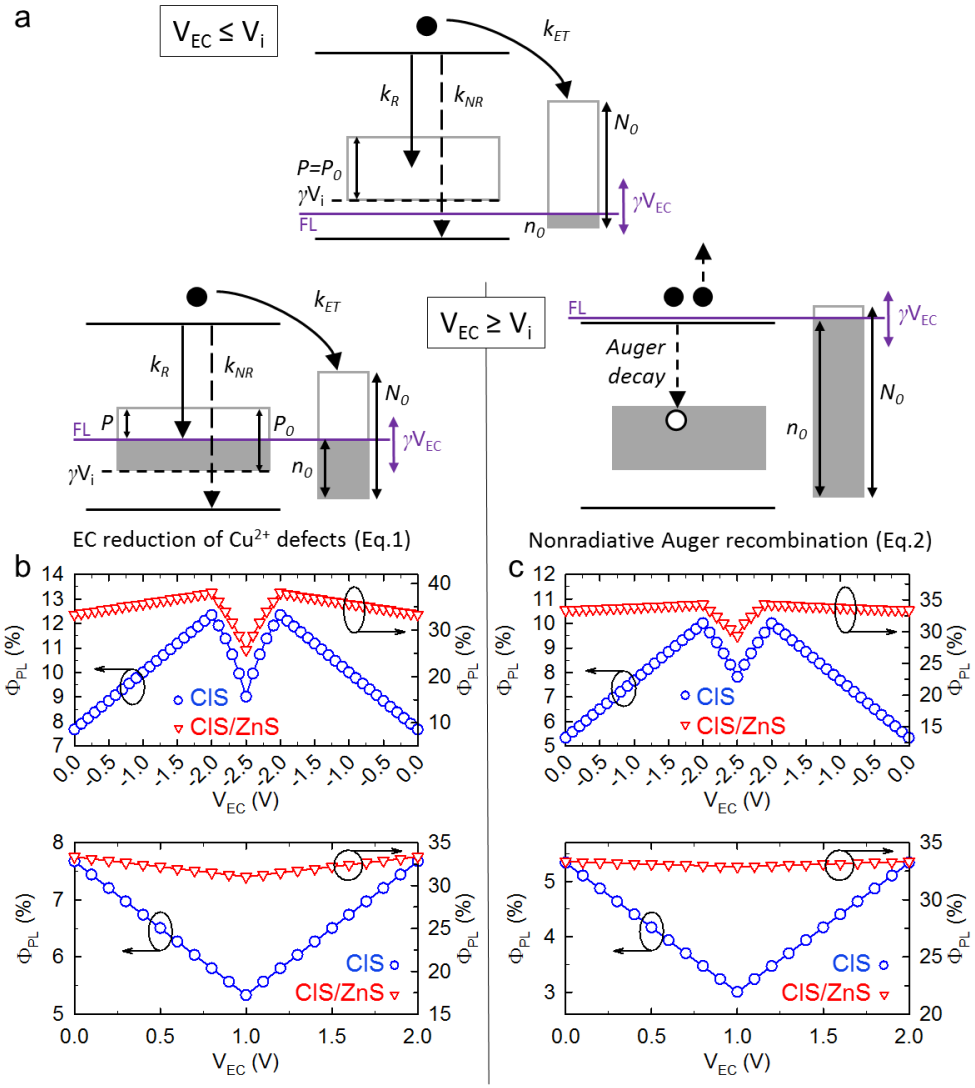

Figure 4 *(c) Diagram illustrating the model used to describe the effect of the EC potential on the PL quantum yield of CIS and CIS/ZnS NCs via filling/emptying of carrier traps at the NC surface (right side of the NC). The Fermi level (FL) is depicted as purple line. For negative EC potentials larger than -2.5 V, two scenarios are possible depending on the attenuation factor between the applied potential and the shift of the FL. For high attenuations (γ=5, lower left panel) leading to moderate shift of the NC FL, direct electron injection results in EC conversion of Cu^{2+} defects into less emissive Cu^{+} centers. For negligible attenuation factor (γ=1, lower right panel), the FL reaches the NC conduction band leading to direct injection of electrons in*

the NC quantized states. Activation of nonradiative Auger recombination through the negative trion pathway lowers the PL efficiency. The calculated trends following the different routes of the PL intensity for CIS (blue circles, left y-axes) and CIS/ZnS NCs (red triangles, right y-axes) normalized to their value at V_{EC}=0 for varying negative and positive EC potentials are shown in (b) and (c) respectively.

Given these considerations, the total PL quantum yield can be expressed as

$$\Phi_{PL}(V_{EC}) = \frac{P}{P_0} \cdot \left[F_B \frac{k_{RAD}}{k_{RAD}+ k_{NRAD}} + F_D \frac{k_{RAD}}{k_{RAD}+ k_{NRAD}+ k_{ET}}\right] \quad (2)$$

On the other hand, for negligible attenuation factors, the FL would reach the NC conduction band leading to direct injection of electrons in the NC quantized states (lower right panel in Figure 4a). In this case, the dimming of the PL intensity at high negative potentials is explained by the activation of efficient nonradiative Auger recombination ($\Phi_{AR} \sim 1$)[94] without invoking direct reduction of holelike Cu^{2+} defects to less emissive Cu^{+}. Within this model, the total PL quantum yield can be expressed as

$$\Phi_{PL}(V_{EC}) = \varphi \cdot \left[F_B \frac{k_{RAD}}{k_{RAD}+ k_{NRAD}} + F_D \frac{k_{RAD}}{k_{RAD}+ k_{NRAD}+ k_{ET}}\right] \quad (2)$$

where the term φ is assumed to be unity for $V_{EC} < V_i$, and $\varphi = 1 - \gamma \cdot \beta(V_{EC} - V_i) \cdot \Phi_{AR}$ for $V_{EC} \geq V_i$, which describes the progressive reduction of the population of photoexcited NCs in the ensemble due to the activation of efficient Auger recombination outpacing both radiative decay and electron trapping and thus affecting F_D and F_B equally. It is worth noting that eqs 2 and 3 are equivalent for $V_{EC} < V_i$ and both describe the PL tuning by passivation/activation of surface traps. On the other hand, for $V_{EC} \geq V_i$ the two equations describe the possible quenching mechanisms in two distinct ways.

To illustrate the model, we use both eqs 2 and 3 to calculate the evolution of Φ_{PL} as a function of the EC potential of both CIS and CIS/ZnS NCs using the experimental k_{RAD} and k_{NRAD} and a set of parameters chosen for matching the experimental Φ_{PL}-values of both systems at V_{EC} = 0 V (5% and 35%, respectively, Table S1 and Table S2). The results of the simulations under both negative and positive V_{EC} are reported in Figure 4b,c. Our semiquantitative model, which does not consider voltage-dependent interface polarization or capacitive effects in the multilayer ITO/ZnO/NCs structure leading to nonlinearity in the PL response versus V_{EC}, reproduces the main experimental trends for both samples by taking into consideration that electron trapping is more effective in core-only CIS NCs than in core/shell CIS/ZnS NCs due to the larger number of available surface electron traps in the absence of the wideband-gap shell. According to both equations, upon applying a negative V_{EC}, the progressive filling of surface states with electrons increases the fraction of "bright" NCs in the ensemble, leading to a two-fold enhancement of Φ_{PL} of CIS NCs, for which electron trapping dominates the exciton decay process at V_{EC} = 0 V. On the other hand, the PL efficiency of CIS/ZnS NCs is essentially unaltered by the EC potential, which is in

agreement with the experimental data in Figure 1 and 3, and confirms that the wide-band-gap shell renders the majority of NCs in the ensemble "bright". When $V_{EC} \geq V_i$, Φ_{PL} of both samples decreases. In the case of $\gamma = 5\ V^{-1}$, corresponding to strong attenuation of the EC potential (lower left panel in Figure 4a,b), eq 2 predicts the progressively lower availability of intragap holelike Cu^{2+} centers upon direct electron injection, which outpaces the brightening effect due to suppressed surface electron trapping and affects "bright" and "dark" NCs subpopulations equally. Such trend further indicates that the Cu^{2+} states in each NC have nearly the same energy. On the other hand, for $\gamma = 1\ V^{-1}$, corresponding to no attenuation of the EC potential (lower right panel in Figure 4a,c), eq 3 describes the observed dimming by activation of ultrafast Auger recombination through the negative trion pathway, lowering the overall population of emitting NCs. The model also reproduces the modulation of the PL intensity at positive V_{EC}, where a progressively lowered Fermi level activates electron traps in CIS NCs to a greater degree than in the core/shell system.

Conclusions. In summary, we combined temperature controlled PL and SEC experiments to investigate the recombination mechanisms in ternary CIS NCs. PL experiments as a function of temperature reveal that electron trapping at surface defects is not a temperature-activated process. On the other hand, intrinsic nonradiative decay, which competes with radiative capture of the CB electron by intragap Cu-related defects, is thermally activated and can be suppressed by cooling samples down to cryogenic temperatures. This channel is independent of the quality of surface passivation and is possibly associated with internal electron accepting defects. Tuning the Fermi level by the application of an EC potential modifies the occupancy of the intragap electron traps (likely surface related), which leads to pronounced changes in the emission intensity of core-only CIS NCs. The effects of the EC potential are less pronounced in CIS/ZnS NCs due to the reduced abundance of intragap defects. Both systems show darkening at high negative EC potentials without modifications of the respective PL decay dynamics. This effect can be explained by electron injection into the NC CB leading to activation of nonradiative Auger recombination. An alternative (or additional) mechanism for PL quenching under high negative V_{EC} is EC conversion of Cu^{2+} defects into Cu^{1+} species that are less emissive due to the need for capturing a photoexcited hole from the NC valence band, which competes with fast hole trapping by nonemissive defects activated at high Fermi levels.

Methods. Synthesis of CIS and CIS/ZnS NCs. The CIS used in this study were synthesized following the procedure described in ref 74. Typically, copper(I) iodide and indium(III) acetate were dissolved in a mixture of 1-dodecanethiol (DDT) and oleylamine (OLA) in a round-bottomed flask, and the mixture was degassed for 30 min. The reaction flask was then heated to 230 °C for ∼30 min. The ZnS shell of CIS/ZnS NCs has been grown through exposure of the CIS NCs to a solution of zinc oleate at elevated temperature, which formed the shell by cation exchange. Spectroscopic Studies. Absorption spectra of NCs in solution were measured with a Cary 50 UV−vis spectrophotometer. Steady-state PL measurements were performed by exciting samples at 3.06 eV with picosecond-pulsed diode lasers. The emitted light was dispersed with a spectrometer and detected with a charged-coupled device (CCD). Transient PL measurements were carried out using ∼70 ps pulses at 3.06 eV from a pulsed diode laser (Picoquant LDH-P series). The emitted light was collected with a photomultiplier coupled to time-correlated single-photon counting unit (time resolution ∼600 ps). Temperature-dependent PL and transient PL measurements were carried out on NC thin films drop-casted on quartz substrates and mounted inside a cryostat with optical access. PLE measurements were conducted using a xenon lamp dispersed by a double grating monochromator (Gemini, Jobin Yvonne) and the PL spectra were collected with a liquid nitrogen-cooled CCD camera coupled to a Jobin Yvonne Triax monochromator.

Spectro-electrochemical Measurements. Indium tin oxide (ITO) coated glass slides (50 × 7 × 0.7 mm, R_S < 100 Ω) were purchased from Delta Technologies (Part No. CG-90IN-CUV). The ITO coated surface was first covered with zinc oxide (ZnO) nanoparticles (NP) (Nanograde, ~50 nm diameter) to avoid quenching of NC emission by fast charge/energy-transfer to ITO. The ZnO NP layer (~60 nm thick, as measured using a Dektak profilometer) was deposited by dip-coating the glass/ ITO substrate into an ethanol suspension of ZnO NPs (2 mg/mL, one dip for 10 s) and annealed at 150 °C for 10 min in a nitrogen glovebox. To test the stability of the glass/ITO/ZnO NP substrates during the potential scans, we performed control experiments in which we monitored changes in optical absorption spectra for prolonged exposures to negative and positive potentials. The results of these measurements indicate that the substrates are unaffected by either positive or negative electrochemical potentials for exposure times of tens of minutes, which are much longer than the measurement time used in our SEC experiments (~300 s).

The NCs were deposited onto the ZnO NP layer as a fewmonolayer thick film by dip-coating from a dilute hexane solution (optical density of 0.07 at 500 nm; 2 dips for 10 s). The ITO was connected as a working electrode to the potentiostat (Bio Logic SP-200 Research grade Potentiostat/Galvanostat) and the film was placed into a quartz cuvette filled with the electrolyte (0.1 M tetrabutylammonium perchlorate, $TBAClO_4$, in propylene carbonate). Silver and platinum wires were used as quasi-reference and counter electrodes, respectively. All potentials reported in this work are measured relative to the quasi-reference silver electrode during staircase voltammetry scans (30 s per scan).

ACKNOWLEDGMENT

V.P. and M.L. contributed equally to this work. Financial support from Fondazione Cariplo is acknowledged by S.B. and F.M. through Grant 2012-0844. M.L. thanks the Fondazione Cassa di Risparmio di Tortona for support. S.B. wishes to thank the European Community's Seventh Framework Programme (FP7/2007-2013) under Grant Agreement 324603 for financial support (EDONHIST). H.M. acknowledges support of the Center for Advanced Solar Photophysics (CASP), an Energy Frontier Research Center funded by the U.S. Department of Energy, Office of Science, Basic Energy Sciences. V.I.K. is supported by the Chemical Sciences, Biosciences and Geo sciences Division, Office of Basic Energy Sciences, Office of Science, U.S. Department of Energy.

REFERENCES

(1) Pietryga, J. M.; Park, Y.-S.; Lim, J.; Fidler, A. F.; Bae, W. K.; Brovelli, S.; Klimov, V. I. Chem. Rev. 2016, 116, 10513−10622.
(2) Mashford, B. S.; Stevenson, M.; Popovic, Z.; Hamilton, C.; Zhou, Z.; Breen, C.; Steckel, J.; Bulovic, V.; Bawendi, M.; Coe-Sullivan, S.; Kazlas, P. T. Nat. Photonics 2013, 7, 407−412.
(3) Dai, X.; Zhang, Z.; Jin, Y.; Niu, Y.; Cao, H.; Liang, X.; Chen, L.; Wang, J.; Peng, X. Nature 2014, 515, 96−99.
(4) Klimov, V. I.; Mikhailovsky, A. A.; Xu, S.; Malko, A.; Hollingsworth, J. A.; Leatherdale, C. A.; Eisler, H. J.; Bawendiz, M. G. Science 2000, 290, 314−317.
(5) Gur, I.; Fromer, N. A.; Geier, M. L.; Alivisatos, A. P. Science 2005, 310, 462−465.
(6) Sargent, E. H. Nat. Photonics 2012, 6, 133−135.
(7) Lorenzon, M.; Pinchetti, V.; Bruni, F.; Bae, W. K.; Meinardi, F.; Klimov, V. I.; Brovelli, S. Nano Lett. 2017, 17, 1071.
(8) Lorenzon, M.; Christodoulou, S.; Vaccaro, G.; Pedrini, J.; Meinardi, F.; Moreels, I.; Brovelli, S. Nat. Commun. 2015, 6, 6434. (9) Alivisatos, P. Nat. Biotechnol. 2004, 22, 47−52.
(10) Bruni, F.; Pedrini, J.; Bossio, C.; Santiago-Gonzalez, B.; Meinardi, F.; Bae, W. K.; Klimov, V. I.; Lanzani, G.; Brovelli, S. Adv. Funct. Mater. 2016, 27, 1605533.
(11) Zhong, H.; Zhou, Y.; Ye, M.; He, Y.; Ye, J.; He, C.; Yang, C.; Li, Y. Chem. Mater. 2008, 20, 6434−6443.
(12) Allen, P. M.; Bawendi, M. G. J. Am. Chem. Soc. 2008, 130, 9240− 9241.
(13) Singh, A.; Coughlan, C.; Milliron, D. J.; Ryan, K. M. Chem. Mater. 2015, 27, 1517−1523.
(14) Kolny-Olesiak, J.; Weller, H. ACS Appl. Mater. Interfaces 2013, 5, 12221−12237.
(15) Booth, M.; Brown, A. P.; Evans, S. D.; Critchley, K. Chem. Mater. 2012, 24, 2064−2070.
(16) Li, L.; Pandey, A.; Werder, D. J.; Khanal, B. P.; Pietryga, J. M.; Klimov, V. I. J. Am. Chem. Soc. 2011, 133, 1176−1179. (17) Berends, A. C.; Rabouw, F. T.; Spoor, F. C. M.; Bladt, E.; Grozema, F. C.; Houtepen, A. J.; Siebbeles, L. D. A.; de Mello Donega, C. J. Phys. Chem. Lett. 2016, 7, 3503−3509.
(18) Meinardi, F.; McDaniel, H.; Carulli, F.; Colombo, A.; Velizhanin, K. A.; Makarov, N. S.; Simonutti, R.; Klimov, V. I.; Brovelli, S. Nat. Nanotechnol. 2015, 10, 878.
(19) Yarema, O.; Bozyigit, D.; Rousseau, I.; Nowack, L.; Yarema, M.; Heiss, W.; Wood, V. Chem. Mater. 2013, 25, 3753−3757. (20) Zhong, H.; Lo, S. S.; Mirkovic, T.; Li, Y.; Ding, Y.; Li, Y.; Scholes, G. D. ACS Nano 2010, 4, 5253−5262.
(21) Jana, A.; Lawrence, K. N.; Teunis, M. B.; Mandal, M.; Kumbhar, A.; Sardar, R. Chem. Mater. 2016, 28, 1107−1120.

(22) Speranskaya, E. S.; Beloglazova, N. V.; Abe, S.; Aubert, T.; Smet,́ P. F.; Poelman, D.; Goryacheva, I. Y.; De Saeger, S.; Hens, Z. Langmuir 2014, 30, 7567−7575.
(23) Deng, D.; Chen, Y.; Cao, J.; Tian, J.; Qian, Z.; Achilefu, S.; Gu, Y. Chem. Mater. 2012, 24, 3029−3037.
(24) Yu, K.; Ng, P.; Ouyang, J.; Zaman, M. B.; Abulrob, A.; Baral, T. N.; Fatehi, D.; Jakubek, Z. J.; Kingston, D.; Wu, X.; Liu, X.; Hebert, C.; Leek, D. M.; Whitfield, D. M. ACS Appl. Mater. Interfaces 2013, 5, 2870−2880.
(25) Pons, T.; Pic, E.; Lequeux, N.; Cassette, E.; Bezdetnaya, L.; Guillemin, F.; Marchal, F.; Dubertret, B. ACS Nano 2010, 4, 2531− 2538.
(26) Song, W.-S.; Yang, H. Chem. Mater. 2012, 24, 1961−1967. (27) Sun, C.; Zhang, Y.; Wang, Y.; Liu, W.; Kalytchuk, S.; Kershaw, S. V.; Zhang, T.; Zhang, X.; Zhao, J.; Yu, W. W.; Rogach, A. L. Appl. Phys. Lett. 2014, 104, 261106.
(28) McDaniel, H.; Fuke, N.; Makarov, N. S.; Pietryga, J. M.; Klimov, V. I. Nat. Commun. 2013, 4, 2887.
(29) McDaniel, H.; Fuke, N.; Pietryga, J. M.; Klimov, V. I. J. Phys. Chem. Lett. 2013, 4, 355−361.
(30) Halpert, J. E.; Morgenstern, F. S. F.; Ehrler, B.; Vaynzof, Y.; Credgington, D.; Greenham, N. C. ACS Nano 2015, 9, 5857−5867.
(31) Li, W.; Pan, Z.; Zhong, X. J. Mater. Chem. A 2015, 3, 1649−1655.
(32) Panthani, M. G.; Akhavan, V.; Goodfellow, B.; Schmidtke, J. P.; Dunn, L.; Dodabalapur, A.; Barbara, P. F.; Korgel, B. A. J. Am. Chem. Soc. 2008, 130, 16770−16777.
(33) Li, L.; Coates, N.; Moses, D. J. Am. Chem. Soc. 2010, 132, 22−23.
(34) Arici, E.; Sariciftci, N. S.; Meissner, D. Adv. Funct. Mater. 2003, 13, 165−171.
(35) Knowles, K. E.; Kilburn, T. B.; Alzate, D. G.; McDowall, S.; Gamelin, D. Chem. Commun. 2015, 51, 9129.
(36) Hu, X.; Kang, R.; Zhang, Y.; Deng, L.; Zhong, H.; Zou, B.; Shi, L.- J. Opt. Express 2015, 23, A858−A867.
(37) Brandt, R. E.; Stevanovic, V.; Ginley, D. S.; Buonassisi, T.́ MRS Commun. 2015, 5, 265−275.
(38) Bradshaw, L. R.; Knowles, K. E.; McDowall, S.; Gamelin, D. R. Nano Lett. 2015, 15, 1315−1323.
(39) Meinardi, F.; Ehrenberg, S.; Dhamo, L.; Carulli, F.; Mauri, M.; Bruni, F.; Simonutti, R.; Kortshagen, U.; Brovelli, S. Nat. Photonics 2017, 11, 177−185.
(40) Whitham, P. J.; Marchioro, A.; Knowles, K. E.; Kilburn, T. B.; Reid, P. J.; Gamelin, D. R. J. Phys. Chem. C 2016, 120, 17136−17142.
(41) Zang, H.; Li, H.; Makarov, N. S.; Velizhanin, K. A.; Wu, K.; Park, Y.-S.; Klimov, V. I. Nano Lett. 2017, 17, 1787.
(42) Rice, W. D.; McDaniel, H.; Klimov, V. I.; Crooker, S. A. J. Phys. Chem. Lett. 2014, 5, 4105−4109.
(43) Shabaev, A.; Mehl, M. J.; Efros, A. L. Phys. Rev. B: Condens. Matter Mater. Phys. 2015, 92, 035431.
(44) Knowles, K. E.; Hartstein, K. H.; Kilburn, T. B.; Marchioro, A.; Nelson, H. D.; Whitham, P. J.; Gamelin, D. R. Chem. Rev. 2016, 116, 10820−10851.
(45) Zhong, H.; Bai, Z.; Zou, B. J. Phys. Chem. Lett. 2012, 3, 3167− 3175.
(46) Castro, S. L.; Bailey, S. G.; Raffaelle, R. P.; Banger, K. K.; Hepp, A. F. J. Phys. Chem. B 2004, 108, 12429−12435.
(47) Tran, T. K. C.; Le, Q. P.; Nguyen, Q. L.; Li, L.; Reiss, P. Adv. Nat. Sci.: Nanosci. Nanotechnol. 2010, 1, 025007.

(48) Shi, A.; Wang, X.; Meng, X.; Liu, X.; Li, H.; Zhao, J. J. Lumin. 2012, 132, 1819−1823.
(49) Kim, Y. K.; Ahn, S. H.; Chung, K.; Cho, Y. S.; Choi, C. J. J. Mater. Chem. 2012, 22, 1516−1520.
(50) Sun, J.; Ikezawa, M.; Wang, X.; Jing, P.; Li, H.; Zhao, J.; Masumoto, Y. Phys. Chem. Chem. Phys. 2015, 17, 11981−11989.
(51) Leach, A. D. P.; Shen, X.; Faust, A.; Cleveland, M. C.; La Croix, A. D.; Banin, U.; Pantelides, S. T.; Macdonald, J. E. J. Phys. Chem. C 2016, 120, 5207−5212.
(52) Chen, B.; Zhong, H.; Zhang, W.; Tan, Z. a.; Li, Y.; Yu, C.; Zhai, T.; Bando, Y.; Yang, S.; Zou, B. Adv. Funct. Mater. 2012, 22, 2081−2088.
(53) Uehara, M.; Watanabe, K.; Tajiri, Y.; Nakamura, H.; Maeda, H. J. Chem. Phys. 2008, 129, 134709.
(54) Jara, D. H.; Stamplecoskie, K. G.; Kamat, P. V. J. Phys. Chem. Lett. 2016, 7, 1452−1459.
(55) Brovelli, S.; Galland, C.; Viswanatha, R.; Klimov, V. I. Nano Lett. 2012, 12, 4372−4379.
(56) Viswanatha, R.; Brovelli, S.; Pandey, A.; Crooker, S. A.; Klimov, V. I. Nano Lett. 2011, 11, 4753−4758.
(57) Zhang, W.; Lou, Q.; Ji, W.; Zhao, J.; Zhong, X. Chem. Mater. 2014, 26, 1204−1212.
(58) Stouwdam, J. W.; Janssen, R. A. J. Adv. Mater. 2009, 21, 2916− 2920.
(59) Pandey, A.; Brovelli, S.; Viswanatha, R.; Li, L.; Pietryga, J. M.; Klimov, V. I.; Crooker, S. A. Nat. Nanotechnol. 2012, 7, 792−797.
(60) Meulenberg, R. W.; van Buuren, T.; Hanif, K. M.; Willey, T. M.; Strouse, G. F.; Terminello, L. J. Nano Lett. 2004, 4, 2277−2285.
(61) Erwin, S. C.; Zu, L. J.; Haftel, M. I.; Efros, A. L.; Kennedy, T. A.; Norris, D. J. Nature 2005, 436, 91−94.
(62) Corrado, C.; Hawker, M.; Livingston, G.; Medling, S.; Bridges, F.; Zhang, J. Z. Nanoscale 2010, 2, 1213.
(63) Stringfellow, G. B.; Bube, R. H. Phys. Rev. 1968, 171, 903−915.
(64) Broser, I.; Schulz, H. J. J. Electrochem. Soc. 1961, 108, 545−548.
(65) Peka, P.; Schulz, H. J. Phys. B 1994, 193, 57−65.
(66) Grandhi, G. K.; Tomar, R.; Viswanatha, R. ACS Nano 2012, 6, 9751−9763.
(67) Grandhi, G. K.; Viswanatha, R. J. Phys. Chem. Lett. 2013, 4, 409− 415.
(68) Santiago-Gonzalez, B.; Monguzzi, A.; Pinchetti, V.; Casu, A.;́ Prato, M.; Lorenzi, R.; Campione, M.; Chiodini, N.; Santambrogio, C.; Meinardi, F.; Manna, L.; Brovelli, S. ACS Nano 2017, 7, 6877−6887.
(69) Knowles, K. E.; Nelson, H. D.; Kilburn, T. B.; Gamelin, D. R. J. Am. Chem. Soc. 2015, 137, 13138−13147.
(70) Srivastava, B. B.; Jana, S.; Pradhan, N. J. Am. Chem. Soc. 2011, 133, 1007−1015.
(71) Jaffe, J. E.; Zunger, A. Phys. Rev. B: Condens. Matter Mater. Phys. 1984, 29, 1882−1906.
(72) Jaffe, J. E.; Zunger, A. Phys. Rev. B: Condens. Matter Mater. Phys. 1983, 28, 5822−5847.
(73) Jaffe, J. E.; Zunger, A. Phys. Rev. B: Condens. Matter Mater. Phys. 1983, 27, 5176−5179.
(74) McDaniel, H.; Koposov, A. Y.; Draguta, S.; Makarov, N. S.; Pietryga, J. M.; Klimov, V. I. J. Phys. Chem. C 2014, 118, 16987−16994.
(75) De Trizio, L.; Prato, M.; Genovese, A.; Casu, A.; Povia, M.; Simonutti, R.; Alcocer, M. J. P.; D'Andrea, C.; Tassone, F.; Manna, L. Chem. Mater. 2012, 24, 2400−2406.
(76) Witt, E.; Kolny-Olesiak, J. Chem. - Eur. J. 2013, 19, 9746−9753.

(77) Zhang, S. B.; Wei, S.-H.; Zunger, A.; Katayama-Yoshida, H. Phys. Rev. B: Condens. Matter Mater. Phys. 1998, 57, 9642−9656.
(78) Tang, X.; Cheng, W.; Choo, E. S. G.; Xue, J. Chem. Commun. 2011, 47, 5217−5219.
(79) Kraatz, I. T.; Booth, M.; Whitaker, B. J.; Nix, M. G. D.; Critchley, K. J. Phys. Chem. C 2014, 118, 24102−24109.
(80) Liu, W.; Zhang, Y.; Zhao, J.; Feng, Y.; Wang, D.; Zhang, T.; Gao, W.; Chu, H.; Yin, J.; Wang, Y.; Zhao, J.; Yu, W. W. J. Lumin. 2015, 162, 191−196.
(81) Galland, C.; Ghosh, Y.; Steinbrueck, A.; Sykora, M.; Hollingsworth, J. A.; Klimov, V. I.; Htoon, H. Nature 2011, 479, 203−207.
(82) Jha, P. P.; Guyot-Sionnest, P. ACS Nano 2009, 3, 1011−1015. (83) Xie, R.; Rutherford, M.; Peng, X. J. Am. Chem. Soc. 2009, 131, 5691−5697.
(84) Wuister, S. F.; de Mello Donega, C.; Meijerink, A. J. Phys. Chem. B 2004, 108, 17393−17397.
(85) Xu, Y.; Schoonen, M. A. A. Am. Mineral. 2000, 85, 543−556. (86) Johnson, B.; Korte, L.; Lußky, T.; Klaer, J.; Lauermann, I. J. Appl. Phys. 2009, 106, 073712.
(87) Jasieniak, J.; Califano, M.; Watkins, S. E. ACS Nano 2011, 5, 5888−5902.
(88) Chung, H.; Choi, H.; Kim, D.; Jeong, S.; Kim, J. J. Phys. Chem. C 2015, 119, 7517−7524.
(89) Ridley, B. K. Quantum Processes in Semiconductors; Oxford University Press, 1999.
(90) Jha, P. P.; Guyot-Sionnest, P. J. Phys. Chem. C 2010, 114, 21138− 21141.
(91) Lorenzon, M.; Sortino, L.; Akkerman, Q.; Accornero, S.; Pedrini, J.; Prato, M.; Pinchetti, V.; Meinardi, F.; Manna, L.; Brovelli, S. Nano Lett. 2017, 17, 3844.
(92) Jin, S.; Song, N.; Lian, T. ACS Nano 2010, 4, 1545−1552.
(93) Dewald, J. F. J. Phys. Chem. Solids 1960, 14, 155−161.
(94) Makarov, N. S.; McDaniel, H.; Fuke, N.; Robel, I.; Klimov, V. I. J. Phys. Chem. Lett. 2014, 5, 111−118.
(95) Brovelli, S.; Bae, W. K.; Meinardi, F.; Santiago Gonzalez, B.;́ Lorenzon, M.; Galland, C.; Klimov, V. I. Nano Lett. 2014, 14, 3855− 3863.
(96) Bozyigit, D.; Yarema, O.; Wood, V. Adv. Funct. Mater. 2013, 23, 3024−3029.
(97) Rowland, C. E.; Currie, M.; Susumu, K.; Oh, E.; Kushto, G.; Efros, A. L.; Huston, A. H.; Delehanty, J. B. Opt. Mater. Express 2017, 7, 1871− 1881.